Hindawi
Shock and Vibration
Volume 2023, Article ID 6616922, 15 pages
https://doi.org/10.1155/2023/6616922

*Research Article*

# Multiple Time-Scales Analysis to Predict the Quasiperiodic Oscillatory Response of a Thin-Walled Beam Subjected to 1: 1: 1 Simultaneous Resonance

**Ali Kandil**[1,2], **Y. S. Hamed**[3], **Jan Awrejcewicz**[4] and **Nasser A. Saeed**[2,4,5]

[1]*Department of Applied and Computational Mathematics, Institute of Basic and Applied Sciences, Egypt-Japan University of Science and Technology (E-JUST), New Borg El-Arab City 21934, Alexandria, Egypt*
[2]*Department of Physics and Engineering Mathematics, Faculty of Electronic Engineering, Menoufia University, Menouf 32952, Egypt*
[3]*Department of Mathematics and Statistics, College of Science, Taif University, P.O. Box 11099, Taif 21944, Saudi Arabia*
[4]*Department of Automation, Biomechanics, and Mechatronics, Faculty of Mechanical Engineering, Lodz University of Technology, Lodz 90924, Poland*
[5]*Mathematics Department, Faculty of Science, Galala University, Galala City 43511, Egypt*

Correspondence should be addressed to Nasser A. Saeed; nasser.a.saeed@el-eng.menofia.edu.eg

Received 23 July 2023; Revised 6 September 2023; Accepted 7 September 2023; Published 20 September 2023

Academic Editor: Arturo Garcia-Perez



This paper introduces a study on the horizontal and vertical deflections of the cross section of a thin-walled rotating beam. These deflections are governed by a system of two ordinary differential equations in order to describe their Cartesian directions. Based on multiple time-scales analysis, truncated asymptotic expansions are assumed to be approximate solutions to the given problem. Furthermore, an extracted autonomous system of differential equations governs the change rate of the amplitudes and phases of the beam deflections. The beam's rotation speed is adjusted to be in the neighborhood of both of the natural frequencies of the deflections such that the beam is subjected to 1: 1: 1 simultaneous resonance. A stability test is conducted according to the first method of Lyapunov in order to determine whether the equilibrium point is asymptotically stable or not. The beam's deflections turn unstable once its speed is in the neighborhood of its modal natural frequencies. There exists a multistable solution at some values of the beam's speed depending on the hysteresis manner of the model according to forward or backward sweeping of this speed. Furthermore, a range of centrifugal forces of the rotating hub can make the beam's deflections exhibit quasiperiodic responses which are confirmed by time response, orbital map, and amplitude spectrum. Eventually, some remarks are recommended for the external excitation frequency in order that the beam stays in the periodic behavior.

## 1. Introduction

The response periodicity of mechanical vibratory applications has attracted much attention from many researchers all over the world. These applications might exhibit periodic behaviors, but also there might be quasiperiodic or chaotic behaviors. These nonperiodic behaviors can harm or destroy the mechanical structure due to the disability of predicting such behaviors. A thin-walled rotating beam is a type of these applications that should be examined. Yao et al. [1] have built their research on analyzing the dynamical behavior of a thin-walled rotating beam subjected to an overheated supersonic gas burst. They represented the beam's deflections by partial differential equations according to Hamilton's principle. Hence, they discretized such equations into ordinary differential equations according to Galerkin's technique. They concluded the existence of periodic and chaotic motions in the oscillations of the studied beam. Wang and Zhang [2, 3] checked the stability of a rotating blade with variable coefficients where geometric nonlinearities are involved in the motion equation. The multiple time-scales technique was applied in order to

examine the equilibrium solutions' stability and bifurcations of the studied case. They assured the occurrence of bifurcation and multiperiodicity at large average rotating speed or large fluctuating amplitude in case of a nonsmall fluctuation frequency. Sina and Haddadpour [4] considered the axial and torsional deflection of a thin-walled rotating beam subjected to primary and secondary warping with the aid of Hamilton's principle. They predicted the dynamical behavior of this type of structure regarding rotor blades of turbo-machinery where an induced static torque could happen in the presence of pretwist angle and material anisotropy. Pešek et al. [5] modeled and simulated the effect of frictional elements on a rotating blade interaction where the centrifugal force determined the contact force values between the element and the blades. The authors found that the mutual friction had a great effect of mitigating the vibration when the normal forces were beneath radial and axial forces' excitation limits. Zhang and Li [6] studied the dynamics of a predeformed rotating blade subjected to gaseous pressure of harmonic type. Using Lagrange's equations, they obtained the equations of motion and normalized them through dimensionless parameters. It could be explored that both the vibration amplitude and the initial deflection's distribution affected the equilibrium behavior of the predeformed blade. Luo et al. [7] proposed a similar design technique based on the transfer matrix of the stepped thickness and thin plates. They introduced a prototype plate made of steel alloys in order to validate the proposed technique that could predict an accurate dynamical performance of the prototype plate showing an important significance in engineering practice. Kandil and Eissa [8] extended the application of the traditional positive position feedback (PPF) controller in order to improve its performance in controlling the vibrations of a thin-walled beam. They have mitigated the original peaks resulting from the traditional PPF by imposing dual saturation controllers. Asghari and Hashemi [9] built their analysis on the modified couple stress theory in order to analyze the vibrations of the 3D microspinning Rayleigh beams including the rotary inertia and gyroscopic effects based on Hamilton's principle. They showed that the linear and nonlinear natural frequencies had been affected by the length-scale value in addition to the critical spinning speeds of the studied microbeams. Yao et al. [10] focused on the time-varying spinning speed of a rotating beam subjected to supersonic air fluid. They considered the warping effect on the rectangular cross section of the studied beam. They proved the existence of periodic motion and chaotic motion in the oscillations of the rotating blade using bifurcation diagrams and phase portraits. Wang et al. [11] checked the existence of vortices between coupled turbine blades that are rotating with time-varying spinning speeds. A saddle-node bifurcation phenomenon occurred with changing the coupling parameter where this phenomenon could be delayed with increasing the coupling parameter. Zhang et al. [12, 13] investigated the superharmonic and 2: 1 internal resonance cases simultaneously of a rotating beam that was implanted in a strong pressure gaseous environment. Various phenomena were explored such as saturation, jump, and hysteresis in addition to quasiperiodic motion revealed by time responses, phase portraits, and Poincare maps in the studied dynamical model. Niu et al. [14] studied the free vibratory behavior of a rotating FG panel enhanced by graphene platelets where the boundary conditions of the cantilever are assumed. They plotted Campbell diagrams to reveal that the large spinning speed has led to a large stiffness of the studied rotating beam. Gu et al. [15] considered the Coriolis and centrifugal force effects in studying a proposed vibrational rotating beam model where its fabricated material was homogeneous and isotropic using Rayleigh–Ritz method compared to ANSYS software results. The authors reported issues of internal resonance, mode shape shift, frequency veering, and dynamics stiffness effect among modes. Kandil and Kamel [16–18] explored the effect of Hopf points on the stability of time-delayed control of a vibratory rotating beam. They have concluded and plotted Hopf curves in order to give a boundary of the safe stable region of operation. Basta et al. [19] proposed a metamaterial structure which was a rotating beam connected to mass-damper-spring subsystems implemented for vibration mitigation targets. The beam exhibited bifurcation and fluttering once it approached the critical rotational speed while the coupled absorber reduced that speed slightly. Wang et al. [20, 21] included the gravitational and modal interactions that led to 3: 1 internal resonance of a rotating cantilever beam excited by primary or secondary resonance cases. In the primary resonance, the second mode could be stimulated, while in the secondary resonance, the first mode response could be generated. Gu et [22] simplified the mechanism of the air clearance's airflow leakage into the axial excitation where a steady state plus a small periodic perturbed spinning speed were considered as a transversal excitation. They concluded that the oscillations of the $O$, $U$, and $X$ patterns of graphene-cantilever plate have the largest, second-largest, and smallest amplitudes, respectively. Lin et al. [23] dealt with the several modes of an imperfect beam including geometric defects restrained by an elastic root based on Hamilton's principle, the Euler–Bernoulli beam theory, and the differential quadrature method. The results assured that the imperfection mode and the elastic root had significant effect on the regions of instability. Dang et al. [24] presented the temperature rise influence on the dynamical characteristics of a rotating beam holding barrier coatings subjected to transversal harmonic forces. The research indicated that the softening nonlinearity of the studied rotating beam with thermal barrier coatings was enhanced according to the rise of temperature. Hamed and Kandil [25] focused on the time-delay effects of the saturation phenomenon that existed in the control of a vibratory rotating beam. They gave time-delay criteria for a safe system operation in order to exhibit a stable bounded beam's behavior. Quaegebeur et al. [26] studied the internal resonance and its relation to suppressing the oscillations of a cyclically symmetric system with geometric nonlinearities. Through the simulations, the amplitude of excitation reached an effective range within the internal resonance that led to overall vibration suppression. Jokar et al. [27] considered a precone angle in a rotating beam mounted on a rigid hub through Hamilton's principle and the Rayleigh–Ritz method. The beam's temporal

response was affected by the pretwist besides the flap- and edge-wise frequencies that were influenced also by the beam's velocity. Niu et al. [28] developed a rotating composite panel with a graphene material for examining the resonant behavior of such panels subjected to severe excitations and three types of blade thickness. They plotted Campbell diagram in order to show the dangerous rotating speeds and modes. Kloda and Warminski [29] investigated the longitudinal-bending-twisting oscillations of a rotating beam based on the theory of Euler–Bernoulli beam neglecting the shear deformation. The authors proved that the beam's speed and tip-mass loading affected the beam's directional bending where they shifted the resonance curves towards larger frequencies. Song et al. [30] observed (theoretically and experimentally) the aeroengine drum performance with a repetitive rub impact between the stator and the rotor of a rotating shell whose equations of motion were derived in the frame of Lagrange equations. They proposed a suggestion for an efficient guide to design shell thin-walled structures in turbo machinery and aeroengines. Lotfan et al. [31] considered the stiffening and Coriolis effects to build an accurate model of a functionally graded (FG) rotating beam spinning with a time-dependent speed whose derivation was based on the spectral Chebyshev and the multiple time-scales techniques. Zero chord- and flap-wise deformations with static elongation were experienced in the constant speed rotating FG beam. Shenas et al. [32] derived the strain-displacement equations of an FG rotating microbeam according to the von Karman hypothesis along with the modified strain gradient theory. They concluded that the microblades of a rectangular shape had bigger frequencies than those of the trapezoidal shape.

Some other papers discussed the vibrations of thin-walled beams considering the shear deformation. Osmani and Meftah [33] studied the shear deformation effect on the lateral buckling of an elastic tapered thin-walled bisymmetric section beam subjected to axial and bending forces. The real-time lateral buckling resistance of short-tapered box beams was overestimated by the classical solution of simply supported thin-walled beams. Schmidrathner [34] considered the influence of the shear force distribution on the torsional prismatic thin-walled beams using the asymptotic splitting method and Bredt's formulas. The shear force caused cross-sectional deformation, and therefore applying Bredt's formulas was needed for necessity. Latalski and Zulli [35] applied the generalized beam theory on a thin-walled beam whose out-of-plane components were derived from the proposition of Vlasov's internal constraint of shear in-deformable middle surface. They provided the crucial contribution in case of a change in cross section that happened at equilibrium. Sahraei et al. [36] developed a criterion for the statically analyzed thin-walled beams considering asymmetric cross section, global and through-thickness warping, and effects of shear deformation. They showed the effects of partial coupling arising in the cases of doubly, point-, and mono-symmetric sections. Bui et al. [37] proposed a vibration analysis of a laminated thin-walled composite I-beam utilizing the general high-order shear deformation theory for buckling and free-oscillation behaviors based on unified shear strains. Considering additional shear effects in the thin-walled beam theory, the gained results from the higher-order assumptions were lower than those from the classical and first-order assumptions. Banić et al. [38] derived incremental steady-state equations using the Lagrangian formulation and Hooke's law in order to analyze the nonlinear stability of a shear deformable beam of composite-type structures. They confirmed that the derived model could be considered as a shear locking-free model.

Additional research papers studied both isotropic and composite rotating beams. Ghafari and Rezaeepazhand [39] used the Rayleigh–Ritz reduction method to examine a cross-sectional composite beam including the transverse shear deformation effects, coupling stiffness constants, and honeycomb core on different isotropic beams. They discussed reducing the time cost by the studied beam analysis in contrary to the 3D finite element analysis in order to provide a fast and accurate structural optimization. Shevtsov et al. [40] developed an improved structural health monitoring that was acoustic-based where the directivity of waves emitted by the wedge actuators in thin-walled beams were fabricated from plastic materials and polymeric composites. The authors clarified the directivity of the excited actuated waves on the modal natural frequencies of the oscillatory actuator. Le et al. [41] proposed a model of a thin-walled beam including multicellular cross sections with either isotropic or orthotropic materials described by Euler–Bernoulli beam theory. They illustrated the practical capability of thin-walled beams by fluid-structural interaction simulation of a hydrokinetic blade subjected to a field condition. Carrera et al. [42] used Lagrange polynomials in order to study the nonlinear behavior resulting from large displacements and rotations in a thin-walled composite beam under axial loading and different angles of the composite structures. The proposed Carrera unified formulation provided accurate results in investigating the nonlinear behavior of composite, isotropic, and FG beams with axial loading. Ramaprasad et al. [43] showed the torsional warping, warping shear, material coupling, and shear deformation in a thin-walled composite beam used widely in aerospace structures where a unified coupled-field formulation was included. They assured the excellent agreement between their results on the mono-symmetric arbitrary-laminated composite channel and I-section beams under torsional and bending loads and the previously published results. Zhao et al. [44–46] investigated the nonlinear oscillations of suspended cables subjected to primary, superharmonic, and subharmonic exciting forces along with thermal effects. They concluded that the cable's oscillatory amplitude depended sensitively on changing the temperature. They included parameter analyses in order to study the effects of different parameters on the multiplicity of the extracted steady-state solutions. In addition, they examined the coupled dynamics among a suspended cable's modes with observing the effects of damage situations and temperature changes on veering points among the cable's modal natural frequencies.

In this research, we focus on the horizontal and vertical cross-sectional deflections of a thin-walled rotating beam. This nonlinear dynamical system can exhibit fundamental modal deflections in the $x$ and $y$ directions governed by a system of two ordinary differential equations. Truncated asymptotic expansions are assumed as approximate solutions to the given problem. The analysis guides us to an autonomous system of differential equations governing the amplitudes and phases of the beam deflections in case the beam's spinning speed is in the neighborhood of its linearized natural frequency. Additionally, the extracted set of equilibrium points is tested for stability utilizing the first method of Lyapunov in order to determine whether the equilibrium point is asymptotically stable or not.

## 2. Dynamical Analysis on the Beam's Motion

This paper focuses on the horizontal and vertical deflections ($u$ and $v$) of a pretwisted thin-walled rotating beam whose cross-sectional dimensions are $a$ and $b$, thickness $h$, and length $L$, mounted on a rigid hub of radius $R$, as shown in Figure 1. The hub is rotating with a time-varying spinning speed $F = f_0 + f\cos\Omega t$ where $f_0$ is a constant component and $f$ is an amplitude of a harmonic component with angular frequency $\Omega$. The beam's plane of vibration makes an angle $\gamma$ with the plane of rotation as shown. During deriving the equations of motion, some assumptions are taken into account: (1) the geometric dimensions of the beam's cross section remain constant, (2) the ratio between the thickness $h$ and the curvature radius $r$ is $\ll 1$, (3) the transverse shear deformation is neglected to such considered thin-walled beam, and (4) the axial displacement is way less than the planar displacements, so its derivatives can be neglected in the strain-displacement relations. The rotating beam's cross section has local coordinates $(x^p, y^p)$ that can be related to the original coordinates $(x, y)$ via the following relations (keeping in mind that $z^p = z$):

$$x = x^p\cos(\gamma+\beta) - y^p\sin(\gamma+\beta), \tag{1a}$$

$$y = x^p\sin(\gamma+\beta) + y^p\cos(\gamma+\beta), \tag{1b}$$

where the angle $\beta = \beta_0 z/L$ refers to the pretwisting angle all over the beam's length and $\beta_0$ is the pretwisting angle at the tip of the beam.

Utilizing the Hamilton principle in order to derive the beam's motion equations yields

$$\int_0^t (\delta K - \delta U + \delta W)\mathrm{d}t = 0, \tag{2}$$

where $\delta$ is the variation operator, the kinetic energy is $K$, the strain energy is $U$, and the external forces' virtual work is $W$. Substituting the quantities $K$, $U$, and $W$ stated in Reference [1] into equation (2) and simplifying give us

$$\ddot{u} - F^2u - F^2\left[\psi_1u'' + \psi_1'u'\right] + \Gamma u'' - \left[\psi_2v'' - \psi_4u''\right]'' = u'\left[u'u'' + v'v''\right] + \frac{u''}{2}\left[u'^2 + v'^2\right] - \dot{F}[R+z] + P_x, \tag{3a}$$

$$\ddot{v} - F^2\left[\psi_1v'' + \psi_1'v'\right] + \Gamma v'' - \left[\psi_2u'' - \psi_3v''\right]'' = v'\left[u'u'' + v'v''\right] + \frac{v''}{2}\left[u'^2 + v'^2\right] + P_y, \tag{3b}$$

where $\dot{()}$ refers to time-derivative and $()'$ refers to derivative w.r.t. $z$. In addition, the quantities $\psi_1$, $\psi_2$, $\psi_3$, $\psi_4$, $\Gamma$, $P_x$, and $P_y$ were given in Reference [1]. Discretize the partial differential equations in (3a), (3b) using single-mode Galerkin's technique by assuming the functions $u$ and $v$ in the form

$$u = x(t)G(z), \tag{4a}$$

$$v = y(t)G(z), \tag{4b}$$

where $x$ and $y$ are the temporal horizontal and vertical displacements and $G$ is the spatial mode shape solution of the beam's free vibration problem. The single-mode discretization may lead to qualitative and quantitative differences in the computed results. However, it has the fundamental contribution to the oscillatory response of the studied beam model according to the experimental observations [1]. Substituting (4a), (4b) into (3a), (3b), multiplying (3a), (3b) by $G$, and integrating w.r.t. $z$ from 0 to 1 give us the following system of ordinary differential equations:

$$\ddot{x} + 2\epsilon\mu\dot{x} + \omega_1^2x + \epsilon\alpha_1\dot{y} + \epsilon\alpha_{21}y + \epsilon\alpha_3\left[x^3 + xy^2\right] - \epsilon\alpha_{41}x\left[2f_0f\cos(\Omega t) + f^2\cos^2(\Omega t)\right] = \epsilon f\alpha_5\Omega\sin(\Omega t), \tag{5a}$$

$$\ddot{y} + 2\epsilon\mu\dot{y} + \omega_2^2y + \epsilon\alpha_1\dot{x} + \epsilon\alpha_{22}x + \epsilon\alpha_3\left[y^3 + x^2y\right] - \epsilon\alpha_{42}y\left(2f_0f\cos(\Omega t) + f^2\cos^2(\Omega t)\right) = 0, \tag{5b}$$

where $\mu$ represents the presumed small factor due to viscosity, $\omega_1$&$\omega_2$ are the linearized natural frequencies of the two directional deflections, $\alpha_1$&$\alpha_{21}$&$\alpha_{22}$ refer to the factors of linear coupling, $\alpha_3$ refers to the factor of cubic coupling, and $\alpha_{41}$&$\alpha_{42}$&$\alpha_5$ are the factors of the beam's excitation. All of the preceding parameters were given in Reference [1]. A book-keeping perturbation parameter $\epsilon$ is proposed in order to distinguish the present problem (given in (5a), (5b)) from the conservative free problem.

Truncated asymptotic expansions can be supposed as approximate solutions to the problem above as follows [47]:

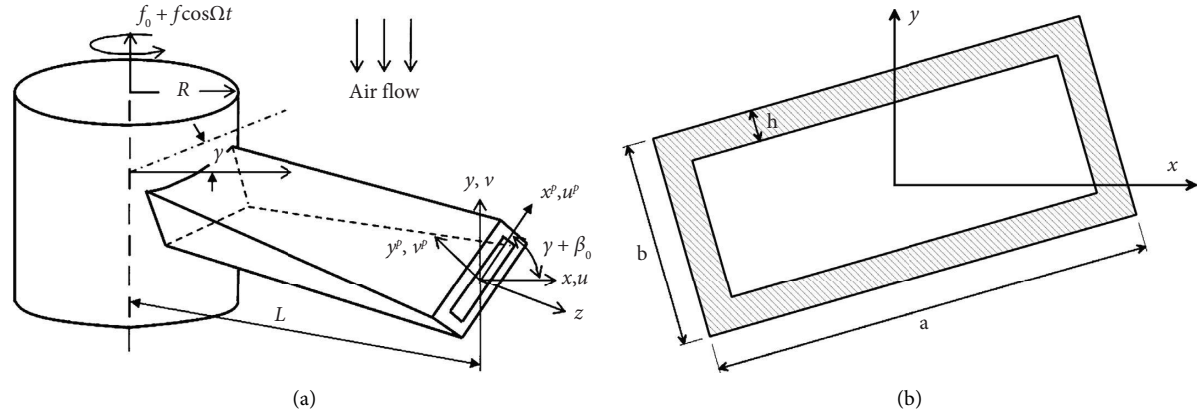


FIGURE 1: (a) Pretwisted thin-walled rotating beam connected to a hub. (b) Cross-sectional view of the beam.

$$x(t) = \sum_{n=0}^{\infty} \epsilon^n x_n \cong x_0 + \epsilon x_1, \tag{6a}$$

$$y(t) = \sum_{n=0}^{\infty} \epsilon^n y_n \cong y_0 + \epsilon y_1, \tag{6b}$$

where $x_n \& y_n$ are the components forming the original $x \& y$, respectively. The time derivatives in (5a), (5b) can also be approximated by new partials derivatives in terms of new time scales $T_0 = t$ and $T_1 = \epsilon t$ as follows:

$$\frac{d}{dt} = \sum_{n=0}^{\infty} \epsilon^n \frac{\partial}{\partial T_n} \cong \frac{\partial}{\partial T_0} + \epsilon \frac{\partial}{\partial T_1}. \tag{7}$$

Substituting (6a), (6b) and (7) into (5a), (5b) and extracting the terms of equal $\epsilon$ (up to $\epsilon^1$) on both sides lead us to the following:

$$\frac{\partial^2 x_0}{\partial T_0^2} + \omega_1^2 x_0 = 0, \tag{8a}$$

$$\frac{\partial^2 y_0}{\partial T_0^2} + \omega_2^2 y_0 = 0, \tag{8b}$$

$$\begin{aligned} \frac{\partial^2 x_1}{\partial T_0^2} + \omega_1^2 x_1 = {} & -2\frac{\partial^2 x_0}{\partial T_0 \partial T_1} - 2\mu\frac{\partial x_0}{\partial T_0} - \alpha_1\frac{\partial y_0}{\partial T_0} - \alpha_{21} y_0 - \alpha_3\left[x_0^3 + x_0 y_0^2\right] \\ & + \alpha_{41} x_0\left[f_0 f\left(e^{i\Omega T_0} + e^{-i\Omega T_0}\right) + \frac{f^2}{4}\left(e^{i\Omega T_0} + e^{-i\Omega T_0}\right)^2\right] - \text{if}\,\frac{\alpha_5\Omega}{2}\left(e^{i\Omega T_0} - e^{-i\Omega T_0}\right), \end{aligned} \tag{8c}$$

$$\begin{aligned} \frac{\partial^2 y_1}{\partial T_0^2} + \omega_2^2 y_1 = {} & -2\frac{\partial^2 y_0}{\partial T_0 \partial T_1} - 2\mu\frac{\partial y_0}{\partial T_0} - \alpha_1\frac{\partial x_0}{\partial T_0} - \alpha_{22} x_0 - \alpha_3\left[y_0^3 + x_0^2 y_0\right] \\ & + \alpha_{42} y_0\left[f_0 f\left(e^{i\Omega T_0} + e^{-i\Omega T_0}\right) + \frac{f^2}{4}\left(e^{i\Omega T_0} + e^{-i\Omega T_0}\right)^2\right]. \end{aligned} \tag{8d}$$

Equations (8a) and (8b) have basic solutions to the conservative free problem as follows:

$$x_0 = A_1 e^{i\omega_1 T_0} + \overline{A}_1 e^{-i\omega_1 T_0}, \tag{9a}$$

$$y_0 = A_2 e^{i\omega_2 T_0} + \overline{A}_2 e^{-i\omega_2 T_0}, \tag{9b}$$

where the integration constants $A_1 \& A_2$ are functions of the second time scale $T_1$, while their conjugates are overbarred. Putting (9a), (9b) into (8c) and (8d) considering the case that the beam's speed is near the $x$ and $y$ linear natural frequencies $\omega_1 \& \omega_2$, i.e., $\Omega \cong \omega_1 \cong \omega_2$, can lead to the following autonomous system of differential equations:

$$\dot{a}_1 = -\mu a_1 - \frac{\alpha_1\omega_2}{2\omega_1}a_2\cos(\phi_1-\phi_2) - \frac{\alpha_{21}}{2\omega_1}a_2\sin(\phi_1-\phi_2) - \frac{\alpha_3}{8\omega_1}a_1a_2^2\sin(2\phi_1-2\phi_2) + \frac{\alpha_{41}f^2}{8\omega_1}a_1\sin(2\phi_1) - \frac{\alpha_5\Omega f}{2\omega_1}\cos\phi_1, \tag{10a}$$

$$a_1\dot{\phi}_1 = \sigma a_1 + \frac{\alpha_1\omega_2}{2\omega_1}a_2\sin(\phi_1-\phi_2) - \frac{\alpha_{21}}{2\omega_1}a_2\cos(\phi_1-\phi_2) - \frac{\alpha_3}{4\omega_1}a_1a_2^2 - \frac{3\alpha_3}{8\omega_1}a_1^3 - \frac{\alpha_3}{8\omega_1}a_1a_2^2\cos(2\phi_1-2\phi_2) + \frac{\alpha_{41}f^2}{8\omega_1}a_1\cos(2\phi_1) + \frac{\alpha_{41}f^2}{4\omega_1}a_1 + \frac{\alpha_5\Omega f}{2\omega_1}\sin\phi_1, \tag{10b}$$

$$\dot{a}_2 = -\mu a_2 - \frac{\alpha_1\omega_1}{2\omega_2}a_1\cos(\phi_1-\phi_2) + \frac{\alpha_{22}}{2\omega_2}a_1\sin(\phi_1-\phi_2) + \frac{\alpha_3}{8\omega_2}a_1^2a_2\sin(2\phi_1-2\phi_2) + \frac{\alpha_{42}f^2}{8\omega_2}a_2\sin(2\phi_2), \tag{10c}$$

$$a_2\dot{\phi}_2 = (\sigma-\sigma_{\text{int}})a_2 - \frac{\alpha_1\omega_1}{2\omega_2}a_1\sin(\phi_1-\phi_2) - \frac{\alpha_{22}}{2\omega_2}a_1\cos(\phi_1-\phi_2) - \frac{\alpha_3}{4\omega_2}a_1^2a_2 - \frac{3\alpha_3}{8\omega_2}a_2^3 - \frac{\alpha_3}{8\omega_2}a_1^2a_2\cos(2\phi_1-2\phi_2) + \frac{\alpha_{42}f^2}{8\omega_2}a_2\cos(2\phi_2) + \frac{\alpha_{42}f^2}{4\omega_2}a_2, \tag{10d}$$

where $\phi_1 = \sigma t - \beta_1$, $\phi_2 = (\sigma - \sigma_{\text{int}})t - \beta_2$, $\sigma = \Omega - \omega_1$, and $\sigma_{\text{int}} = \omega_2 - \omega_1$. The exact solutions of the equilibrium state ($\dot{a}_n = \dot{\phi}_n = 0$) of (10a), (10b), (10c), (10d) cannot be found analytically. Instead, we resort to numerical techniques such as the Newton–Raphson algorithm for predicting the solution and pseudo-arc length for correcting the solution. Also, the extracted set of equilibrium points should be checked for stability utilizing the first method of Lyapunov [47] in order to determine whether the equilibrium point is asymptotically stable or not.

## 3. Graphical Analysis on the Beam's Motion

We are going to describe the nonlinear behavior of the beam's motion due to changing some parameters and show these behaviors graphically via several response curves. The physical constants to be adopted for the operation are as follows: the viscosity coefficient $\mu = 0.02$, the horizontal angular natural frequency $\omega_1 = 120\pi$, the vertical angular natural frequency $\omega_2 \cong \omega_1$, the linear coupling coefficients $\alpha_1 = -0.82$, $\alpha_{21} = -0.003$, $\alpha_{22} = -0.001$, the cubic coupling coefficient $\alpha_3 = 0.9$, the excitation coefficients $\alpha_{41} = 0.55$, $\alpha_{42} = 0.5$, $\alpha_5 = 6.55$, the excitation force amplitudes $f_0 = 7$, $f = [0,10]$, and the beam's spinning speed $\Omega \cong \omega_1$. As you will see in the figures, solid curves refer to stable solutions according to Lyapunov's first method stability criterion. In addition, dashed curves refer to unstable solutions according to the same criterion. Figure 2 shows the graphical interpretation of the beam's horizontal and vertical vibration amplitudes $a_1$&$a_2$ (Figures 2(a) and 2(c)) and phases $\phi_1$&$\phi_2$ (Figures 2(b) and 2(d)) in response to the spinning speed detuning $\sigma$ at $f = 1.0$. It is noticed that the amplitudes and phases turn from stable (solid paths) into unstable (dashed paths) in the $\sigma$-domain of about $[-1.53, +1.55]$. Within the stable $\sigma$-domain, the horizontal amplitude $a_1$ cannot exceed 2 while the vertical amplitude $a_2$ cannot exceed 0.5. Regarding the phases, the horizontal phase $\phi_1$ cannot exceed the range $[-\pi/2, +\pi/2]$ while the vertical phase $\phi_2$ cannot exceed the range $[-0.1, +0.1]$. The separating points between the stable and unstable branches are called Hopf bifurcation points due to the stability criterion of Lyapunov where the system has pure imaginary eigenvalues. We will check for the nonlinear response at different values of $\sigma$ later in this work. Moving to Figure 3, we have plotted the same relation as in Figure 2 but at a higher force amplitude $f = 2.5$. It is clear that the stable branch of the amplitude $a_1$ has risen significantly with increasing $f$, while the stable range of the amplitude $a_2$ has increased slightly in comparison with the amplitudes plotted in Figure 2. About the phases $\phi_1$&$\phi_2$, you can see a slight change in the phase behavior in comparison with the phases plotted in Figure 2. Continuing the scenario of increasing the force amplitude $f$, Figure 4 is plotted to the show the same relations in Figures 2 and 3 but with $f = 5.0$. As you can notice, there is a drastic change in the form of the curves showing the hardening effect for both the amplitudes and phases. In addition, there exists a multistable solution (for example, at $\sigma = 2$) where we have two stable solutions at this value of $\sigma$. The system will obey either one of them depending on the hysteresis manner of the model according to sweeping the parameter $\sigma$ up or down. Also, the system may jump between these two stable solutions depending on the initial conditions. This leads us to the well-known jump phenomenon which may be a problem whether the jump is sharp leading to system damage or destruction. Accordingly, Figure 5 depicts how the beam's amplitudes respond to the spinning speed detuning $\sigma$ when the internal resonance detuning $\sigma_{\text{int}}$ changes from $-0.5$ to 0.5. It can be shown that the parameter $\sigma_{\text{int}}$ can play a role in changing the form of the curves due to the nonlinearity domination as if we are changing the spinning amplitude $f$ (shown in Figure 4). It is

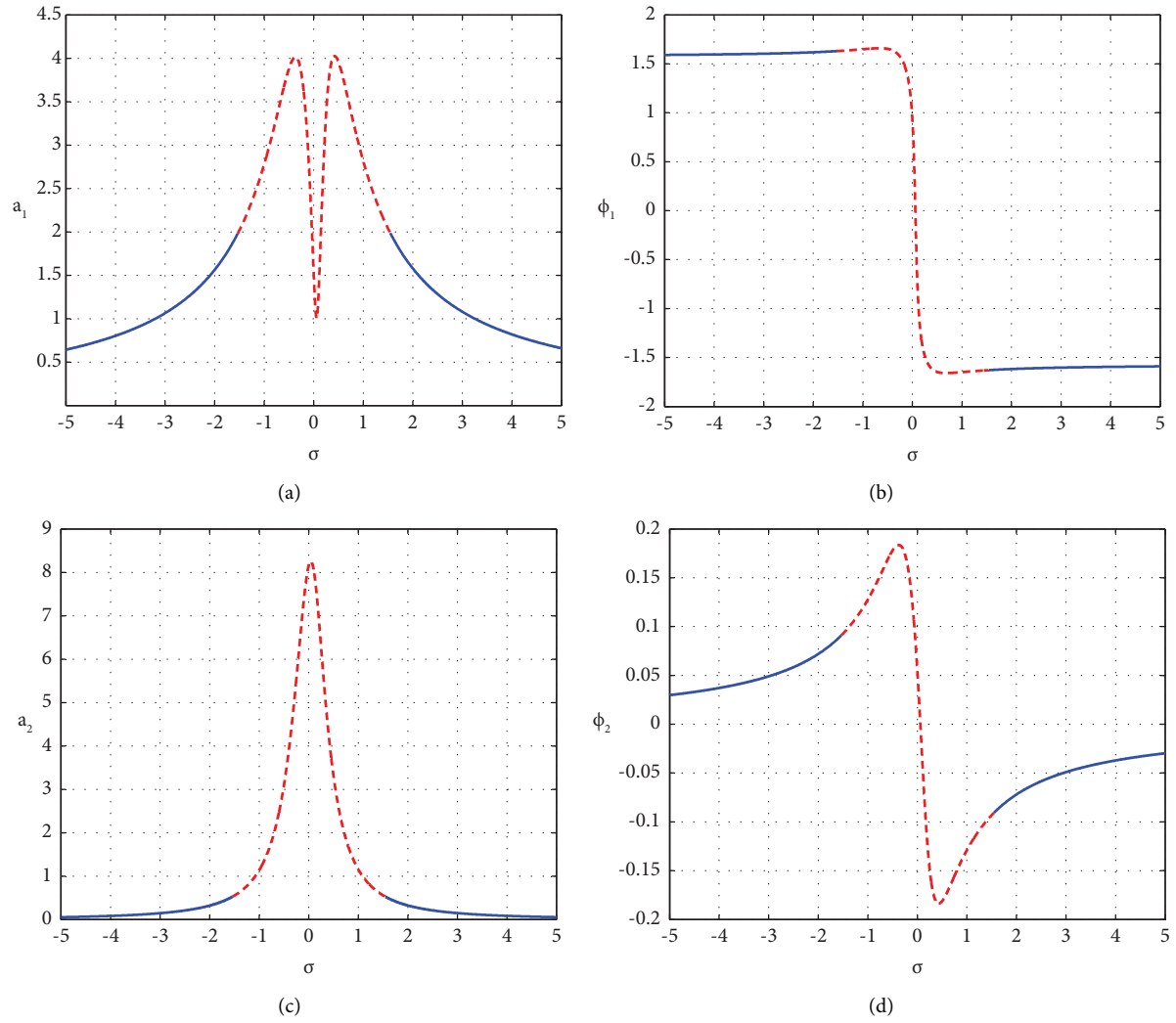


Figure 2: The beam's horizontal and vertical vibration amplitudes $a_1$&$a_2$ (a, c) and phases $\phi_1$&$\phi_2$ (b, d) in response to the spinning speed detuning $\sigma$ at $f = \mathbf{1.0}$.

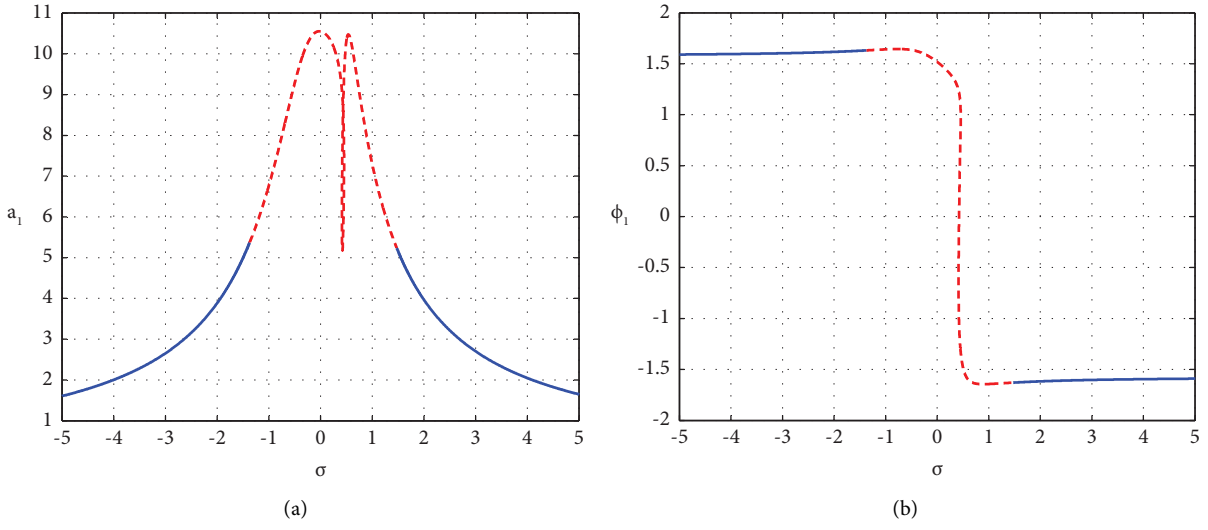


Figure 3: Continued.

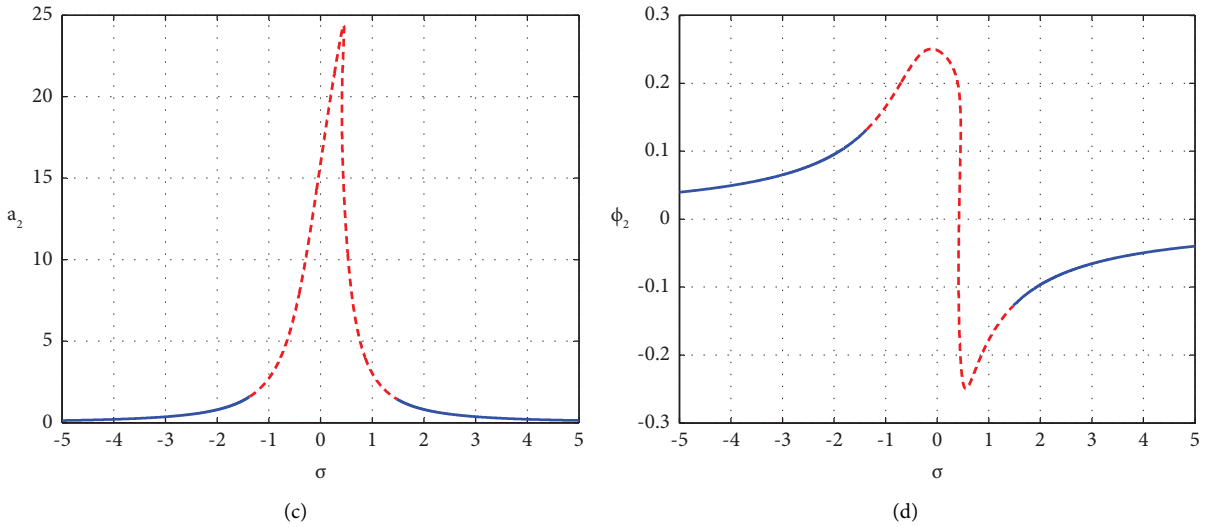


FIGURE 3: The beam's horizontal and vertical vibration amplitudes $a_1$&$a_2$ (a, c) and phases $\phi_1$&$\phi_2$ (b, d) in response to the spinning speed detuning $\sigma$ at $f = \mathbf{2.5}$.

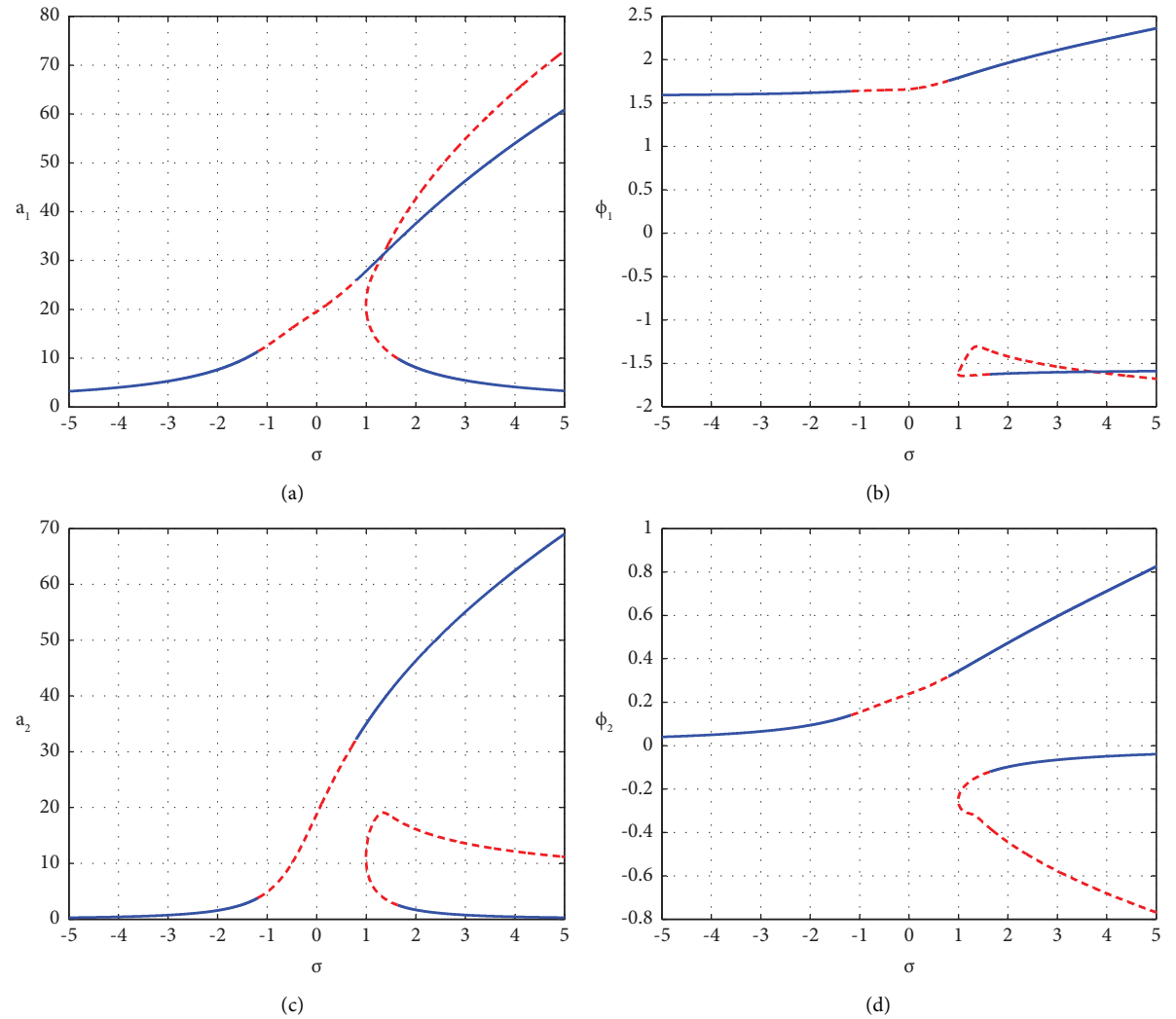


FIGURE 4: The beam's horizontal and vertical vibration amplitudes $a_1$&$a_2$ (a, c) and phases $\phi_1$&$\phi_2$ (b, d) in response to the spinning speed detuning $\sigma$ at $f = \mathbf{5.0}$.

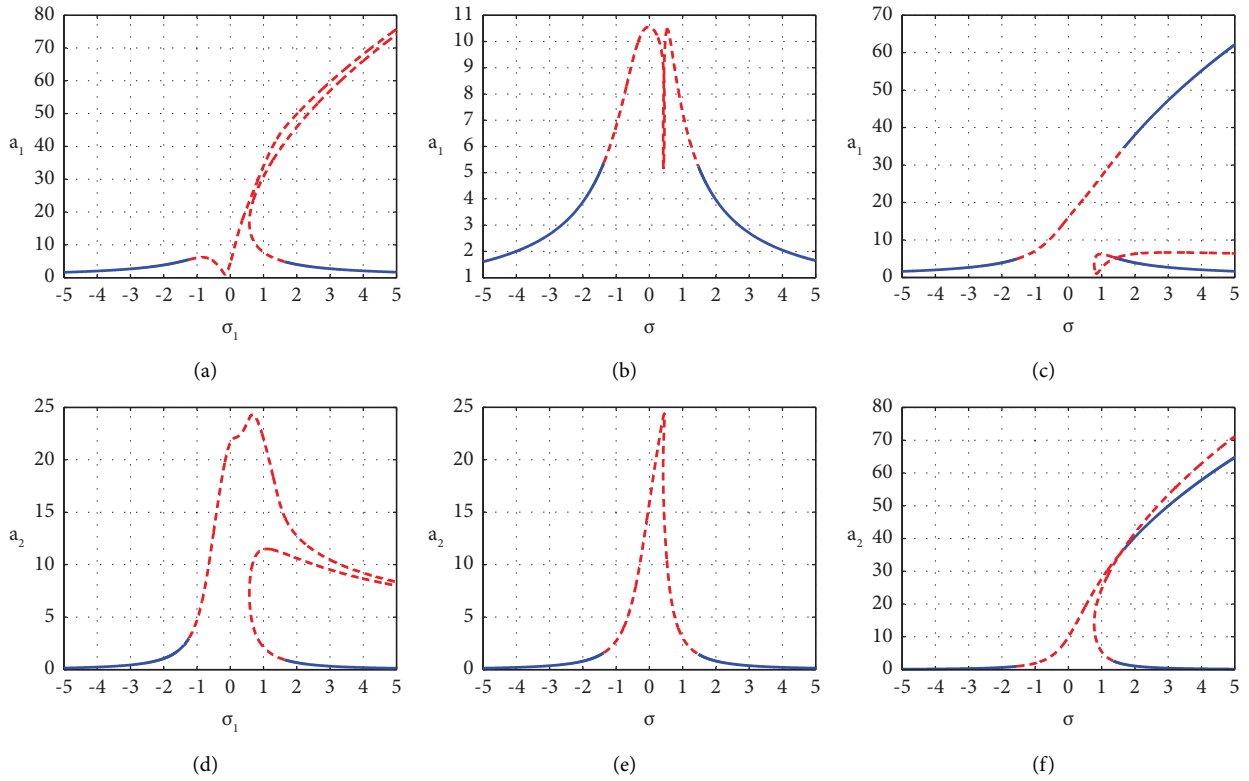


FIGURE 5: The beam's horizontal (a, b, c) and vertical (d, e, f) vibration amplitudes in response to the spinning speed detuning $\sigma$ at $f = \mathbf{2.5}$ and different values of $\sigma_{\mathbf{int}}$: (a, d) $\sigma_{\mathbf{int}} = -\mathbf{0.5}$; (b, e) $\sigma_{\mathbf{int}} = \mathbf{0}$; (c, f) $\sigma_{\mathbf{int}} = +\mathbf{0.5}$.

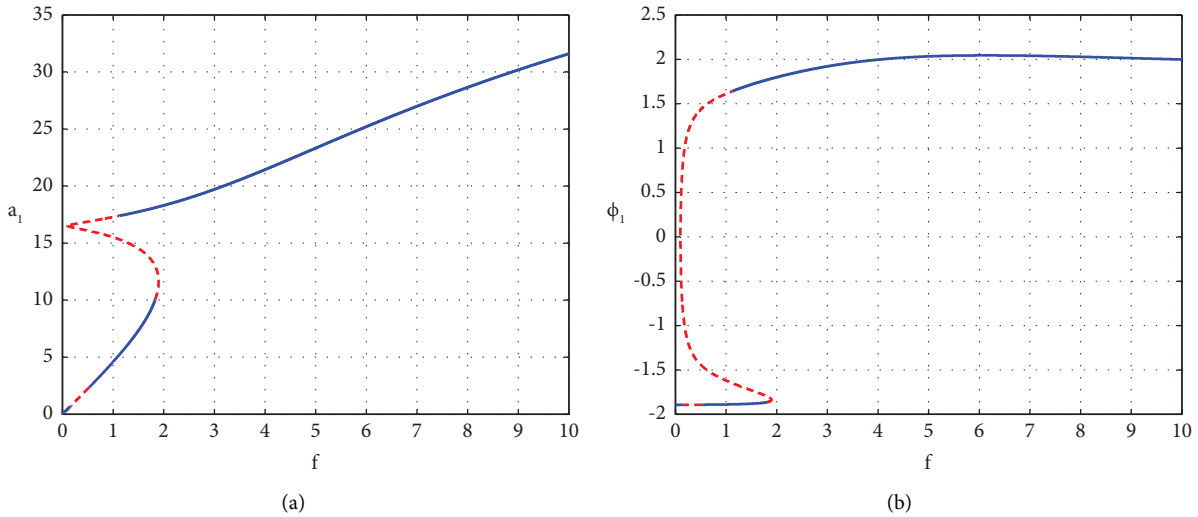


FIGURE 6: Continued.

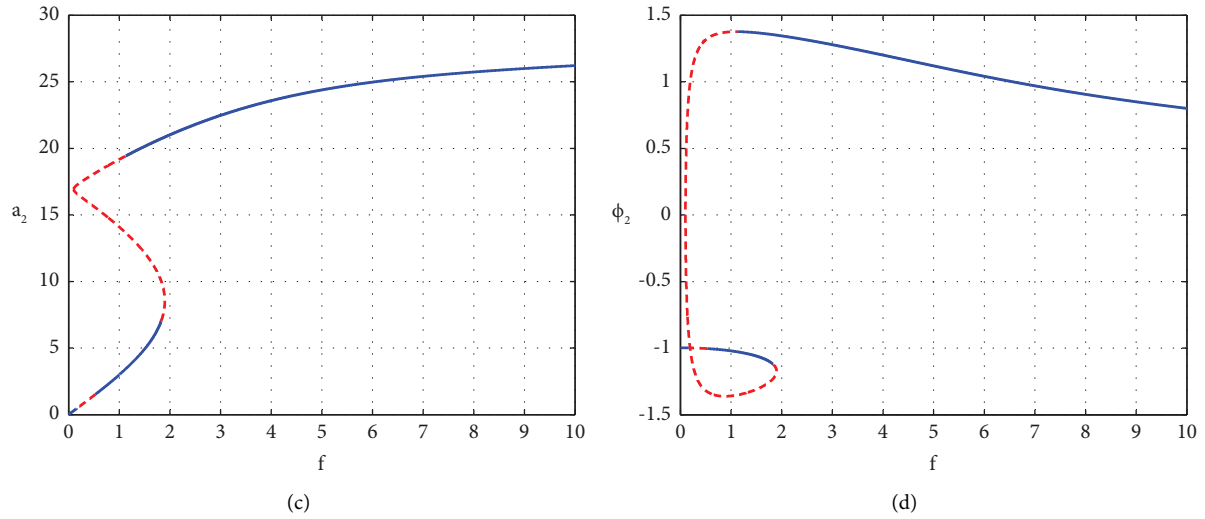


FIGURE 6: The beam's horizontal and vertical vibration amplitudes $a_1$&$a_2$ (a, c) and phases $\phi_1$&$\phi_2$ (b, d) in response to the spinning amplitude $f$ at $\sigma = \mathbf{0.5}$.

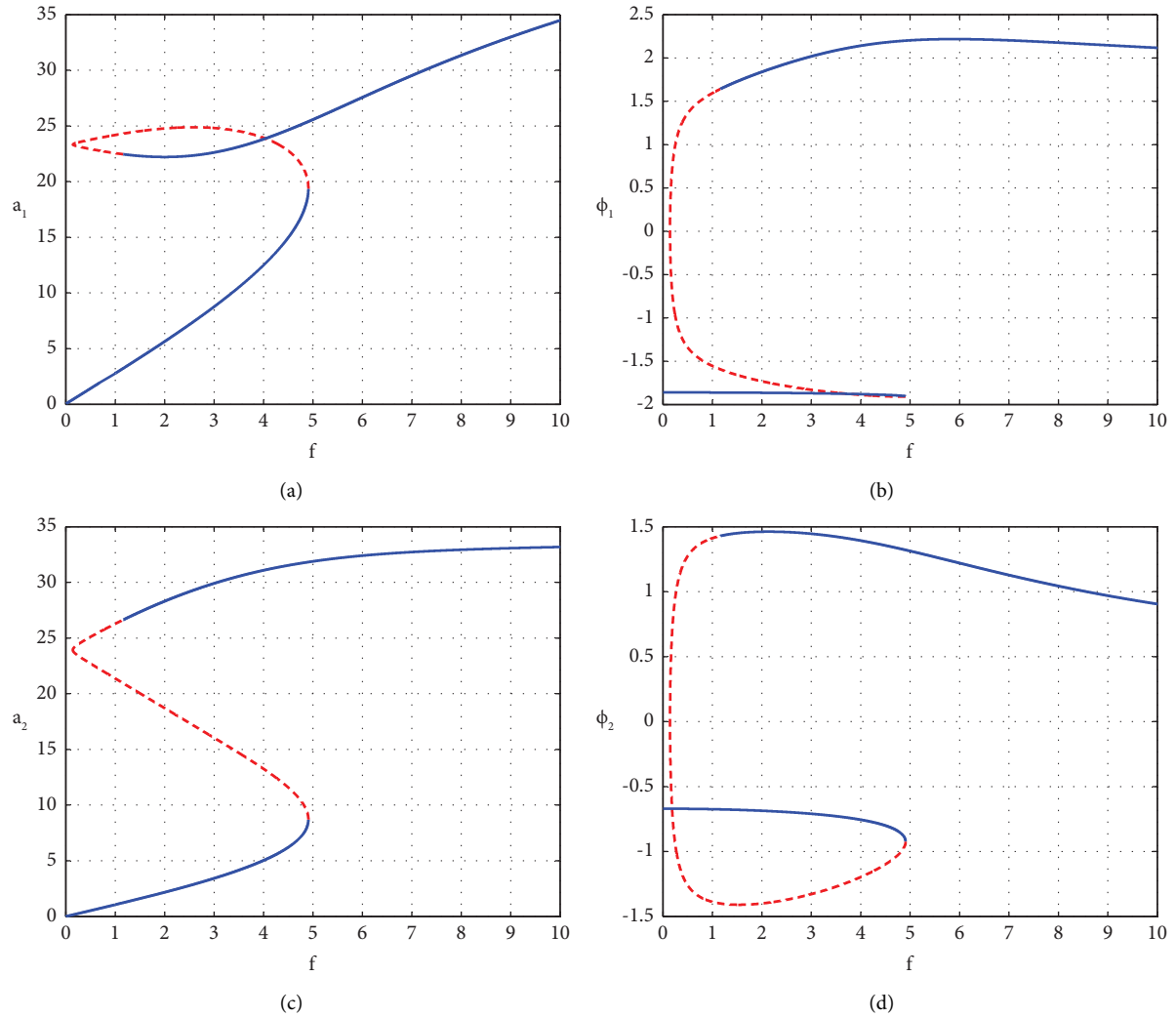


FIGURE 7: The beam's horizontal and vertical vibration amplitudes $a_1$&$a_2$ (a, c) and phases $\phi_1$&$\phi_2$ (b, d) in response to the spinning amplitude $f$ at $\sigma = \mathbf{1.0}$.

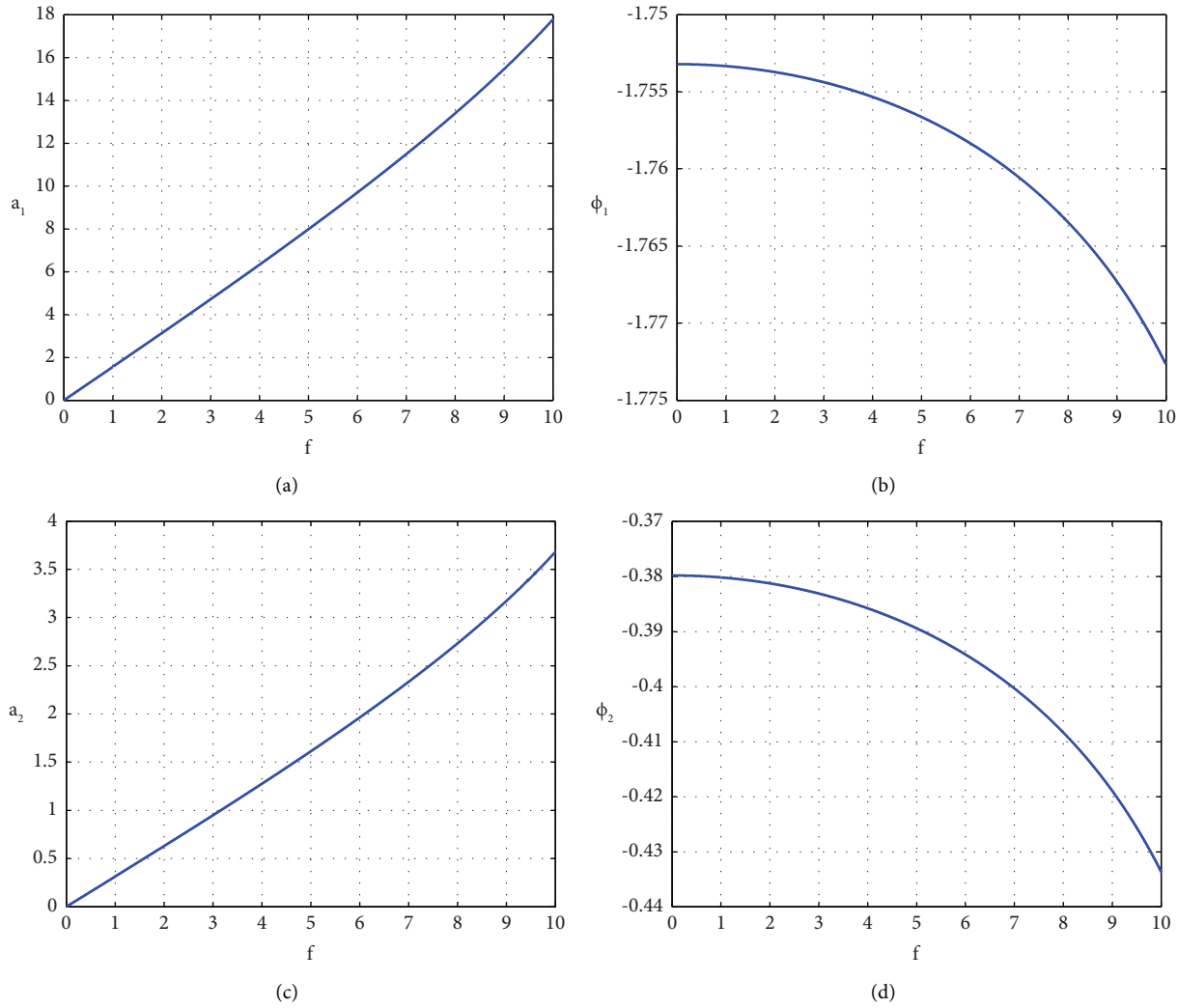


Figure 8: The beam's horizontal and vertical vibration amplitudes $a_1$&$a_2$ (a, c) and phases $\phi_1$&$\phi_2$ (b, d) in response to the spinning amplitude $f$ at $\sigma = \mathbf{2.0}$.

also noted that as $\sigma_{\text{int}}$ deviates from zero, the curves transform from an almost-linear case to a nonlinear case with the existence of multiple solutions (stable or unstable or both).

Contrary to the previous figures, we are moving to another system response in Figure 6 which portrays the beam's horizontal and vertical vibration amplitudes and phases in response to the spinning amplitude $f$ at spinning detuning $\sigma = 0.5$. In Figures 6(a) and 6(c), the very start of the increase of $f$ makes these amplitudes face a Hopf bifurcation point which turns them unstable as shown. Then, facing another Hopf point gets these amplitudes back to the stable state. In this specific $f$-domain, the amplitude $a_1$&$a_2$ may jump to another stable branch depending on the sweeping process or the initial conditions. This multistable solution case is not obvious in this figure but will be discussed later. Increasing $f$ in the same manner makes the amplitudes get bigger as shown. In Figure 7, we have changed the value of $\sigma$ to $\sigma = 1.0$. This change has modified the curves' shape as shown. It is so clear in this figure that the amplitudes may obey one of the multistable solutions in the range $f \in (1, 5)$ depending on the sweeping process or the values of the initial conditions. Afterward, the amplitudes are increasing proportionally with $f$ as pictured. In Figure 8 where $\sigma = 2.0$, the amplitudes respond linearly with $f$, or in other words, there are no multistable branches but only a single stable branch that the system obeys regardless of the sweeping process or the values of the initial conditions. Moreover, Figures 9 and 10 give numerical simulations of the beam's different responses as temporal, orbital, and spectral at $f = 1.0$, $\sigma = 0.0$ (for Figure 9), and $\sigma = 2.0$ (for Figure 10). In Figure 9 where $f = 1.0$ and $\sigma = 0.0$, the beam exhibits quasiperiodic response as shown by the temporal oscillations (horizontal and vertical). In addition, Figure 9(c) clarifies the horizontal-vertical orbitals that are in the form of multilimit cycles denoting the quasiperiodic response. Also, Figures 9(d) and 9(e) picture the horizontal and vertical amplitude spectra where multiple spikes are shown in order to represent the frequencies that form the quasiperiodic response in the studied case. On the other hand, in

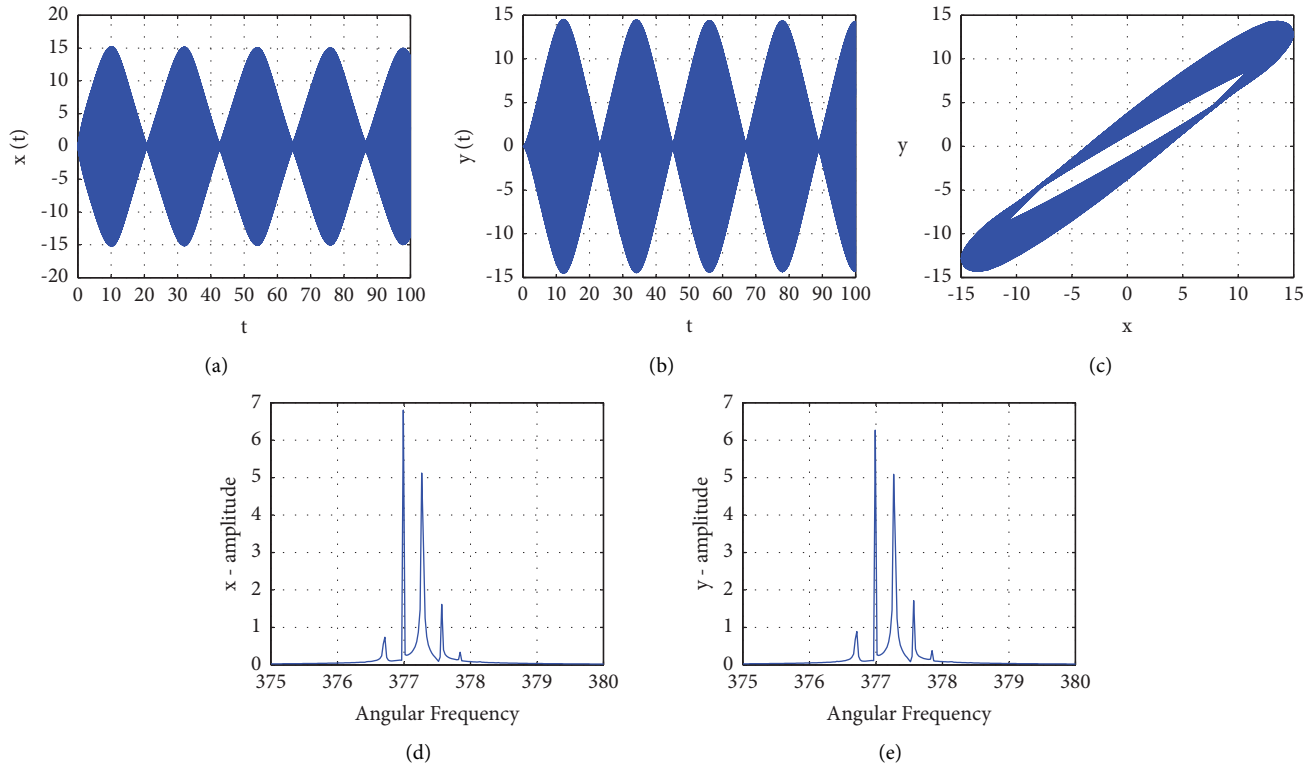


FIGURE 9: The beam's numerical responses at $\sigma = \mathbf{0.0}$ and $f = \mathbf{1.0}$: (a) horizontal time response $x(t)$, (b) vertical time response $y(t)$, (c) horizontal-vertical orbit plot, (d) horizontal amplitude spectrum, and (e) vertical amplitude spectrum.

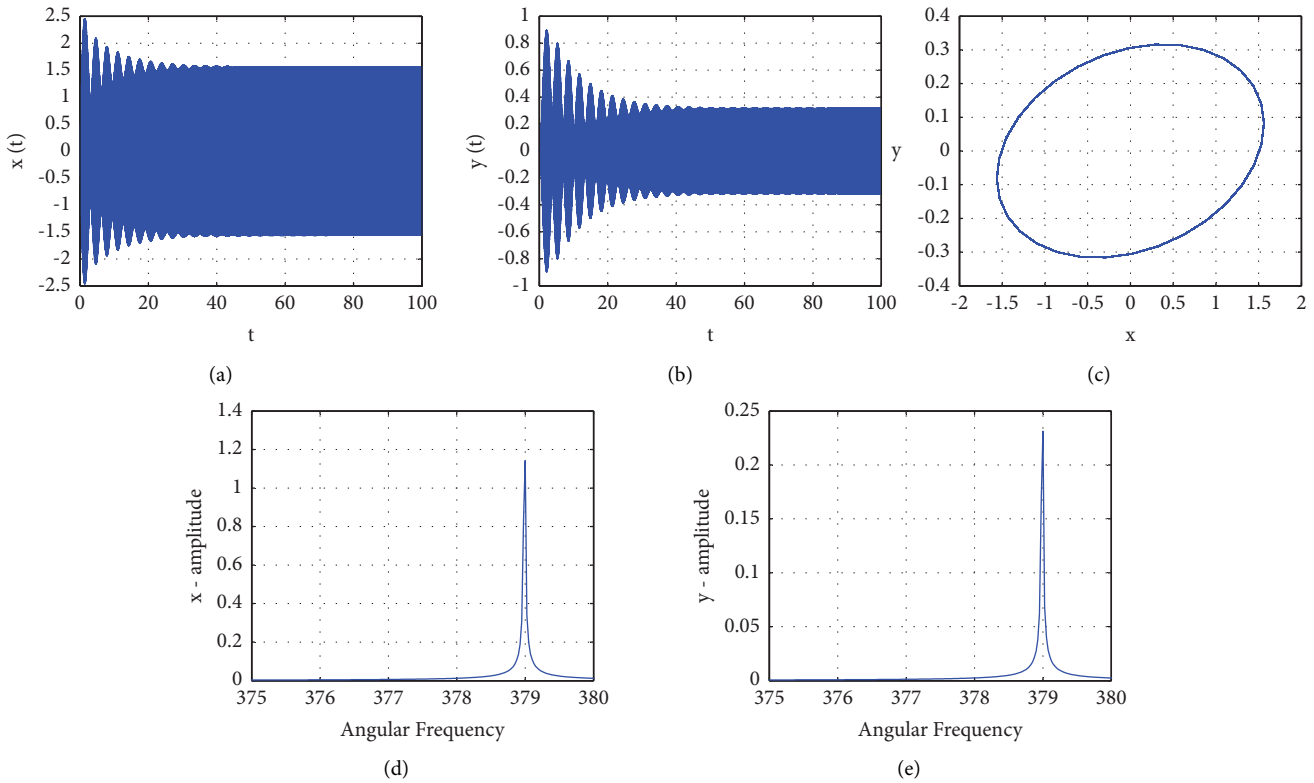


FIGURE 10: The beam's numerical responses at $\sigma = \mathbf{2.0}$ and $f = \mathbf{1.0}$: (a) horizontal time response $x(t)$, (b) vertical time response $y(t)$, (c) horizontal-vertical orbit plot, (d) horizontal amplitude spectrum, and (e) vertical amplitude spectrum.

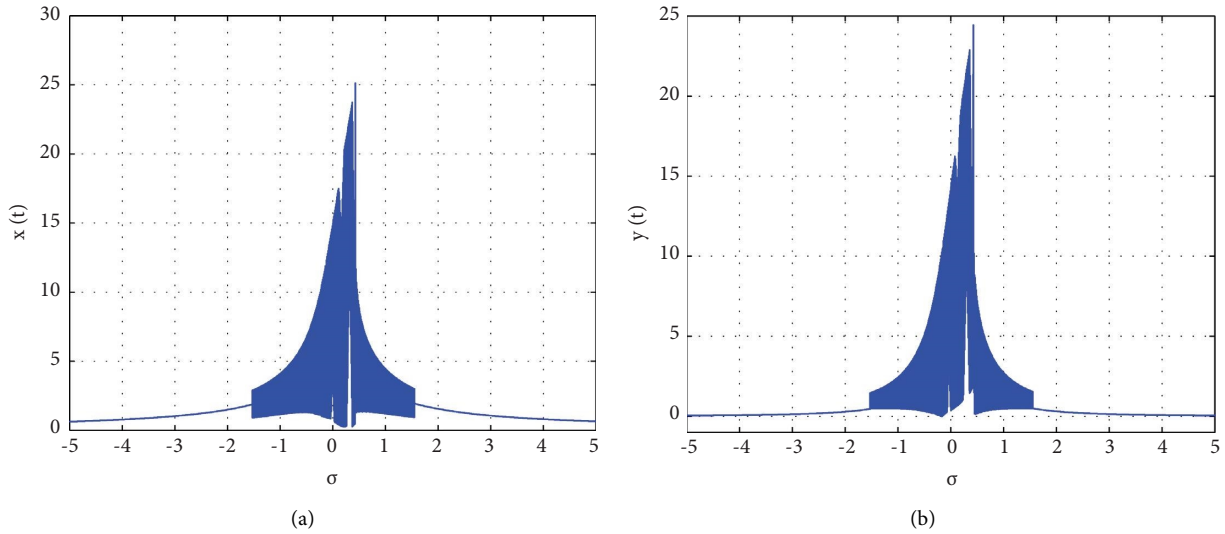


Figure 11: The beam's horizontal (a) and vertical (b) displacement bifurcation behaviors in response to the spinning speed detuning $\sigma$ at $f = \mathbf{1.0}$.

Figure 10, the simulation has been done at $f = 1.0$ and $\sigma = 2.0$ to show the periodic response (unlike the quasiperiodic one in Figure 9) in the temporal oscillations, the orbital plot with single limit cycle, and the amplitude spectra with only a single spike. Figure 11 shows the bifurcation diagram of the beam's horizontal and vertical displacement behaviors in response to the spinning speed detuning $\sigma$ at $f = 1.0$. It is a verification of Figure 2 that the beam exhibits nonperiodic responses if $\sigma$ lies inside the band $[-1.53, +1.55]$.

## 4. Conclusions

In this work, we studied the horizontal and vertical deflections of the cross section of a thin-walled rotating beam. The nonlinear dynamical system of such a beam exhibited fundamental modal deflections in the $x$ and $y$ directions that were governed by a system of two ordinary differential equations. The analysis revealed that the beam's amplitudes and phases turned from a stable state into an unstable state where $\sigma \in [-1.53, +1.55]$. There existed a multistable solution at some values of $\sigma$ depending on the hysteresis manner of the model according to sweeping the parameter $\sigma$ up or down. The very start of increasing $f$ made the stable amplitudes face a Hopf bifurcation point which turned them unstable. Then, facing another Hopf point got these amplitudes back to the stable state. When $\sigma = 0$, the beam exhibited a quasiperiodic response with a multilimit cycle which was assured by time response, orbital map, and amplitude spectrum. Changing to $\sigma = 2.0$ made the beam exhibit a periodic response with a stable limit cycle.

## Data Availability

The data used to support the findings of this study are included within the article.

## Conflicts of Interest

The authors declare that they have no conflicts of interest.

## Authors' Contributions

AK, YH, JA, and NS were responsible for conceptualization, methodology, validation, and review and editing. AK was responsible for software, formal analysis, investigation, original draft preparation, and visualization. All authors have read and agreed to the published version of the manuscript.

## Acknowledgments

The authors would like to acknowledge the Deanship of Scientific Research, Taif University, for funding this work. Also, this work was supported by the Polish National Science Centre, Poland, under the grant OPUS 18 (no. 2019/35/B/ST8/00980).

## References

[1] M. H. Yao, Y. P. Chen, and W. Zhang, "Nonlinear vibrations of blade with varying rotating speed," *Nonlinear Dynamics*, vol. 68, no. 4, pp. 487–504, 2012.

[2] F. Wang and W. Zhang, "Stability analysis of a nonlinear rotating blade with torsional vibrations," *Journal of Sound and Vibration*, vol. 331, no. 26, pp. 5755–5773, 2012.

[3] F. Wang and Y. Qu, "Period doubling motions of a nonlinear rotating beam at 1:1 resonance," *International Journal of Bifurcation and Chaos*, vol. 24, no. 12, Article ID 1450159, 2014.

[4] S. A. Sina and H. Haddadpour, "Axial-torsional vibrations of rotating pretwisted thin walled composite beams," *International Journal of Mechanical Sciences*, vol. 80, pp. 93–101, 2014.

[5] L. Pešek, M. Hajžman, L. Půst, V. Zeman, M. Byrtus, and J. Brůha, "Experimental and numerical investigation of friction element dissipative effects in blade shrouding," *Nonlinear Dynamics*, vol. 79, no. 3, pp. 1711–1726, 2015.

[6] B. Zhang and Y. Li, "Nonlinear vibration of rotating pre-deformed blade with thermal gradient," *Nonlinear Dynamics*, vol. 86, no. 1, pp. 459–478, 2016.

[7] Z. Luo, Y. Zhu, H. Liu, and D. Wang, "Dynamic similitude design method of the distorted model on variable thickness cantilever plates," *Applied Sciences*, vol. 6, no. 8, p. 228, 2016.

[8] A. Kandil and M. Eissa, "Improvement of positive position feedback controller for suppressing compressor blade oscillations," *Nonlinear Dynamics*, vol. 90, no. 3, pp. 1727–1753, 2017.

[9] M. Asghari and M. Hashemi, "The couple stress-based nonlinear coupled three-dimensional vibration analysis of microspinning Rayleigh beams," *Nonlinear Dynamics*, vol. 87, no. 2, pp. 1315–1334, 2017.

[10] M. Yao, L. Ma, and W. Zhang, "Nonlinear dynamics of the high-speed rotating plate," *International Journal of Aerospace Engineering*, vol. 2018, Article ID 5610915, 23 pages, 2018.

[11] D. Wang, Z. Hao, Y. Chen, and Y. Zhang, "Dynamic and resonance response analysis for a turbine blade with varying rotating speed," *Journal of Theoretical and Applied Mechanics*, vol. 56, pp. 31–42, 2018.

[12] B. Zhang, H. Ding, and L. Q. Chen, "Super-harmonic resonances of a rotating pre-deformed blade subjected to gas pressure," *Nonlinear Dynamics*, vol. 98, no. 4, pp. 2531–2549, 2019.

[13] B. Zhang, Y. L. Zhang, X. D. Yang, and L. Q. Chen, "Saturation and stability in internal resonance of a rotating blade under thermal gradient," *Journal of Sound and Vibration*, vol. 440, pp. 34–50, 2019.

[14] Y. Niu, W. Zhang, and X. Y. Guo, "Free vibration of rotating pretwisted functionally graded composite cylindrical panel reinforced with graphene platelets," *European Journal of Mechanics- A: Solids*, vol. 77, Article ID 103798, 2019.

[15] X. J. Gu, Y. X. Hao, W. Zhang, L. T. Liu, and J. Chen, "Free vibration of rotating cantilever pre-twisted panel with initial exponential function type geometric imperfection," *Applied Mathematical Modelling*, vol. 68, pp. 327–352, 2019.

[16] A. Kandil and M. Kamel, "Vibration control of a compressor blade using position and velocity feedback," *Mar*, vol. 24, no. 1, pp. 97–112, 2019.

[17] Y. S. Hamed, A. Kandil, and J. T. Machado, "Utilizing macro fiber composite to control rotating blade vibrations," *Symmetry*, vol. 12, no. 12, Article ID 1984, pp. 1–23, 2020.

[18] A. Kandil, "Study of Hopf curves in the time delayed active control of a 2DOF nonlinear dynamical system," *SN Applied Sciences*, vol. 2, no. 11, p. 1924, 2020.

[19] E. Basta, M. Ghommem, and S. Emam, "Vibration suppression of nonlinear rotating metamaterial beams," *Nonlinear Dynamics*, vol. 101, no. 1, pp. 311–332, 2020.

[20] G. X. Wang, H. Ding, and L. Q. Chen, "Gravitational effects and mode interactions of vertical cantilever beams," *International Journal of Non-linear Mechanics*, vol. 123, Article ID 103493, 2020.

[21] G. X. Wang, H. Ding, and L. Q. Chen, "Dynamic effect of internal resonance caused by gravity on the nonlinear vibration of vertical cantilever beams," *Journal of Sound and Vibration*, vol. 474, Article ID 115265, 2020.

[22] X. J. Gu, W. Zhang, and Y. F. Zhang, "Nonlinear vibrations of rotating pretwisted composite blade reinforced by functionally graded graphene platelets under combined aerodynamic load and airflow in tip clearance," *Nonlinear Dynamics*, vol. 105, no. 2, pp. 1503–1532, 2021.

[23] B. Lin, B. Chen, B. Zhu, J. A. Li, and Y. Li, "Dynamic stability analysis for rotating pre-twisted FG-CNTRC beams with geometric imperfections restrained by an elastic root in thermal environment," *Thin-Walled Structures*, vol. 164, Article ID 107902, 2021.

[24] P. F. Dang, Z. X. Yang, Y. Y. Yan, Q. K. Han, and Z. H. Jin, "Nonlinear vibration characteristics of rotating composite blade considering the temperature-dependent graded material properties," *Composite Structures*, vol. 258, Article ID 113419, 2021.

[25] Y. S. Hamed and A. Kandil, "Influence of time delay on controlling the non-linear oscillations of a rotating blade," *Symmetry*, vol. 13, pp. 85–18, 2021.

[26] S. Quaegebeur, N. Di Palma, B. Chouvion, and F. Thouverez, "Exploiting internal resonances in nonlinear structures with cyclic symmetry as a mean of passive vibration control," *Mechanical Systems and Signal Processing*, vol. 178, Article ID 109232, 2022.

[27] H. Jokar, M. Mahzoon, and R. Vatankhah, "Nonlinear dynamic characteristics of horizontal-axis wind turbine blades including pre-twist," *Ocean Engineering*, vol. 256, Article ID 111441, 2022.

[28] Y. Niu, M. Yao, and Q. Wu, "Resonance in dangerous mode and chaotic dynamics of a rotating pre-twisted graphene reinforced composite blade with variable thickness," *Composite Structures*, vol. 288, Article ID 115422, 2022.

[29] L. Kloda and J. Warminski, "Nonlinear longitudinal–bending–twisting vibrations of extensible slowly rotating beam with tip mass," *International Journal of Mechanical Sciences*, vol. 220, Article ID 107153, 2022.

[30] X. Song, Y. Ren, and Q. Han, "Nonlinear vibration of rotating cylindrical shell due to unilateral contact induced tip rubbing impact: theoretical and experimental verification," *Mechanical Systems and Signal Processing*, vol. 164, Article ID 108244, 2022.

[31] S. Lotfan, M. R. Anamagh, B. Bediz, and E. Cigeroglu, "Nonlinear resonances of axially functionally graded beams rotating with varying speed including Coriolis effects," *Nonlinear Dynamics*, vol. 107, no. 1, pp. 533–558, 2022.

[32] A. G. Shenas, S. Ziaee, and P. Malekzadeh, "Nonlinear free vibration of rotating FG trapezoidal microplates in thermal environment," *Thin-Walled Structures*, vol. 170, Article ID 108614, 2022.

[33] A. Osmani and S. A. Meftah, "Lateral buckling of tapered thin walled bi-symmetric beams under combined axial and bending loads with shear deformations allowed," *Engineering Structures*, vol. 165, pp. 76–87, 2018.

[34] C. Schmidrathner, "Validation of Bredt's formulas for beams with hollow cross sections by the method of asymptotic splitting for pure torsion and their extension to shear force bending," *Acta Mechanica*, vol. 230, no. 11, pp. 4035–4047, 2019.

[35] J. Latalski and D. Zulli, "Generalized beam theory for thin-walled beams with curvilinear open cross-sections," *Applied Sciences*, vol. 10, no. 21, pp. 7802–7818, 2020.

[36] A. Sahraei, P. Pezeshky, S. Sasibut, F. Rong, and M. Mohareb, "Closed form solutions for shear deformable thin-walled beams including global and through-thickness warping effects," *Thin-Walled Structures*, vol. 158, Article ID 107190, 2021.

[37] X. B. Bui, T. K. Nguyen, N. D. Nguyen, and T. P. Vo, "A general higher-order shear deformation theory for buckling

and free vibration analysis of laminated thin-walled composite I-beams," *Composite Structures*, vol. 295, Article ID 115775, 2022.

[38] D. Banić, G. Turkalj, and D. Lanc, "Stability analysis of shear deformable cross-ply laminated composite beam-type structures," *Composite Structures*, vol. 303, Article ID 116270, 2023.

[39] E. Ghafari and J. Rezaeepazhand, "Two-dimensional cross-sectional analysis of composite beams using Rayleigh-Ritz-based dimensional reduction method," *Composite Structures*, vol. 184, pp. 872–882, 2018.

[40] S. Shevtsov, V. Chebanenko, M. Shevtsova, E. Kirillova, and E. Rozhkov, "On the directivity of acoustic waves generated by the angle beam wedge actuator in thin-walled structures," *Actuators*, vol. 8, no. 3, p. 64, 2019.

[41] T. B. Le, A. Christenson, T. Calderer, H. Stolarski, and F. Sotiropoulos, "A thin-walled composite beam model for light-weighted structures interacting with fluids," *Journal of Fluids and Structures*, vol. 95, Article ID 102968, 2020.

[42] E. Carrera, M. D. Demirbas, and R. Augello, "Evaluation of stress distribution of isotropic, composite, and fg beams with different geometries in nonlinear regime via carrera-unified formulation and Lagrange polynomial expansions," *Applied Sciences*, vol. 11, no. 22, Article ID 10627, 2021.

[43] S. Ramaprasad, B. Dattaguru, and G. Singh, "Exact solutions for thin-walled composite open section beams using a unified state space coupled field formulation," *Mechanics Based Design of Structures and Machines*, vol. 51, no. 11, pp. 5983–6007, 2022.

[44] Y. Zhao, H. Lin, L. Chen, and C. Wang, "Simultaneous resonances of suspended cables subjected to primary and super-harmonic excitations in thermal environments," *International Journal of Structural Stability and Dynamics*, vol. 19, no. 12, Article ID 1950155, 2019.

[45] Y. Zhao and I. Gameiro-Ros, "Advances in targeting GIRK channels in disease," *Trends in Pharmacological Sciences*, vol. 42, no. 3, pp. 203–215, 2021.

[46] Y. Zhao, P. Zheng, H. Lin, and L. Chen, "Nonlinear coupled dynamics of suspended cables due to crossover points shifting and symmetry breaking," *European Journal of Mechanics- A: Solids*, vol. 99, Article ID 104921, 2023.

[47] A. H. Nayfeh and D. T. Mook, *Nonlinear Oscillations*, Wiley, New York, NY, USA, 1995.